The effect of conductor permeability on electric current transducers

Cite as: AIP Advances **8**, 047506 (2018); https://doi.org/10.1063/1.4994195
Submitted: 04 July 2017 . Accepted: 31 July 2017 . Published Online: 07 November 2017

M. Mirzaei, P. Ripka, A. Chirtsov, P. Kaspar, and J. Vyhnanek

The effect of conductor permeability on electric current transducers

M. Mirzaei,[1] P. Ripka,[1,a] A. Chirtsov,[1] P. Kaspar,[1] and J. Vyhnanek[1]
[1]*Faculty of Electrical Engineering, Czech Technical University, Technicka 2, 166 27 Praha 6, Czech Republic*

(Received 4 July 2017; accepted 31 July 2017; published online 7 November 2017)

In this paper, experimental works and theoretical analysis are presented to analyze the influence of the conductor permeability on the precision of yokeless current sensors. The results of finite-element method (FEM) fit well the measured field values around the conductor. Finally we evaluate the difference in magnetic fields distribution around non-magnetic and magnetic conductor. The calculated values show that the permeability of the ferromagnetic conductor significally affects the reading of the electric current sensors even at DC. https://doi.org/10.1063/1.4994195

I. INTRODUCTION

Large electric currents are often measured by yokeless current transducers, which have small size and low price and also do not suffer from yoke saturation.[1,2] In the case that the measured current has DC component, Rogowski coil cannot be used and a differential magnetic sensor on the surface of the measured conductor[3] or inside the conductor[4] is typical solution. While for large currents individual discrete sensors are used, small currents up to typically 5 A can be measured by integrated sensors.[5] The main problem of using only two sensors in differential configuration can suppress external homogeneous field, but this configuration has large sensitivity to external currents in any direction.[6] Circular array of DC magnetic sensors is much more effective in this respect.[7] Circular arrays use Hall sensors,[8,9] but these suffer from poor DC stability. AMR sensors have small offset and drift, but due to their small range they can be used only for current sensors up to tens of Amps.[10] Using microfluxgate sensors, the DC stability is good and the current range can be increased to hundreds of Amps.[11]

To our knowledge all published papers on current sensors consider non-magnetic conductor. However, in some applications such as grounding conductors, iron busbars are used for their low price and high robustness. In this paper we study the effect of the busbar permeability on the accuracy of the current transducers. The calculations are done by Finite Element Modeling (FEM). This can be used to optimize the location and number of magnetic sensors to achieve minimum frequency dependence and also minimum influence of external currents. Finite element method (FEM) results are compared with measurements.

II. MODEL CONDUCTOR

In this paper we consider rectangular 30 × 5 mm conductor from soft iron. The conductor hysteresis curve was measured using compensated permeameter. This is an old method which is very useful for this type of materials. For massive soft magnetic materials permeameter gives more precise results than methods using H-coils. The complete hysteresis loop is shown in FIG. 1. The measured electrical conductivity of solid iron rectangular conductor is 5.07 MS/m.

[a]Author to whom correspondence should be addressed. Electronic mail: ripka@fel.cvut.cz

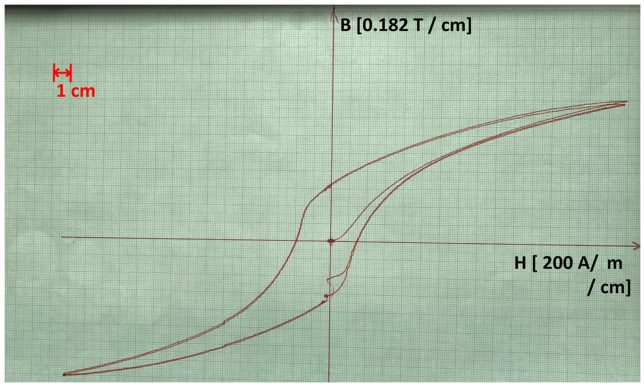

FIG. 1. Measured hysteresis B-H curve.

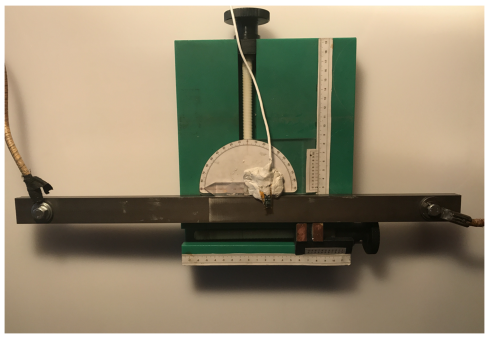

FIG. 2. Experimental setup.

FIG. 2 shows experimental setup for magnetic flux density measurement around solid iron rectangular conductor. Integrated fluxgate sensor DRV425[12] is used for the measurement.

Measurements and calculations of magnetic field around the conductor are done on two paths, which is shown in FIG. 3 as well as conductor dimensions. The distance between x and y paths and the surface of conductor is 1.5 mm. The amplitude of applied current is 23 A for all measurements and simulations.

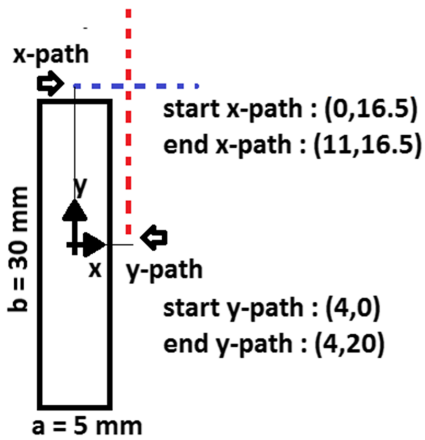

FIG. 3. Considered paths for magnetic flux densities measurement - center of coordinate is located in the center of rectangular conductor.

III. FEM SIMULATIONS AND MEASUREMENTS

FIG. 4 shows DC B-H curve and magnetic relative permeability. The maximum relative magnetic permeability is about 700. The FEM calculations are time harmonic method (FIG. 5), using FEMM package.[13]

Calculated and measured values of magnetic field in the 1.5 mm distance from the conductor are shown in FIGs. 6 and 7. The field sensors will be positioned in the range -2.5 < x < 2.5 mm and -7.5 < y < 7.5 mm. In this range the deviation between the measured and simulated values is below 10%.

The current density distribution in the conductor and magnetic field strength in the conductor and around the conductor are shown in FIGs. 8–10. For DC the current density is constant, while for AC it is affected by the skin effect. Skin effect is increased at higher frequency. Magnetic field distribution is affected both by the current distribution and by the busbar permeability, which is field dependent.

The effects of replacing solid iron conductor with copper conductor on magnetic fields on different paths (FIG. 11) are shown in FIGs. 12–14. It can be seen that largest difference between copper and iron conductors is observed by the sensor located at x=0, which is in the middle of the short side

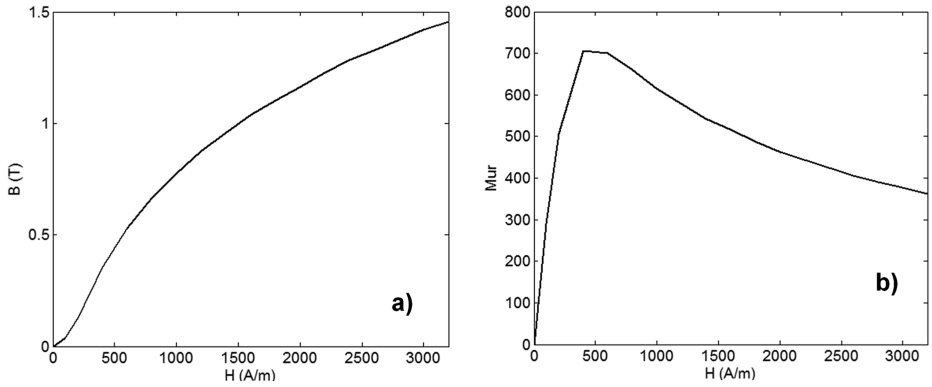

FIG. 4. DC B-H curve (a) and relative magnetic permeability curve (b) extracted from measurement (FIG. 1).

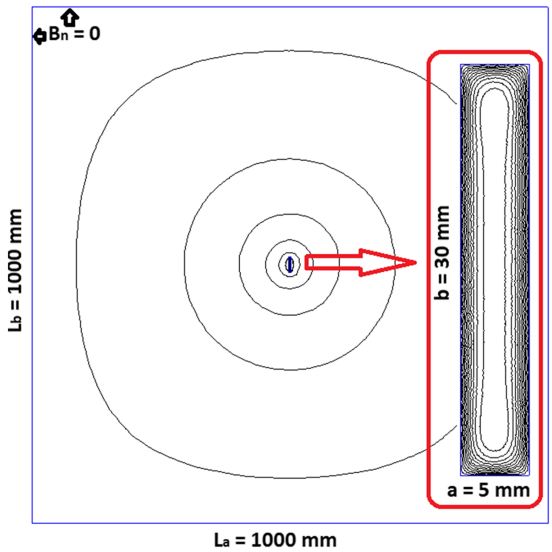

FIG. 5. Magnetic flux distribution using FEM[13] for solid iron rectangular conductor at 50 Hz and boundary conditions with applied current amplitude 23 A.

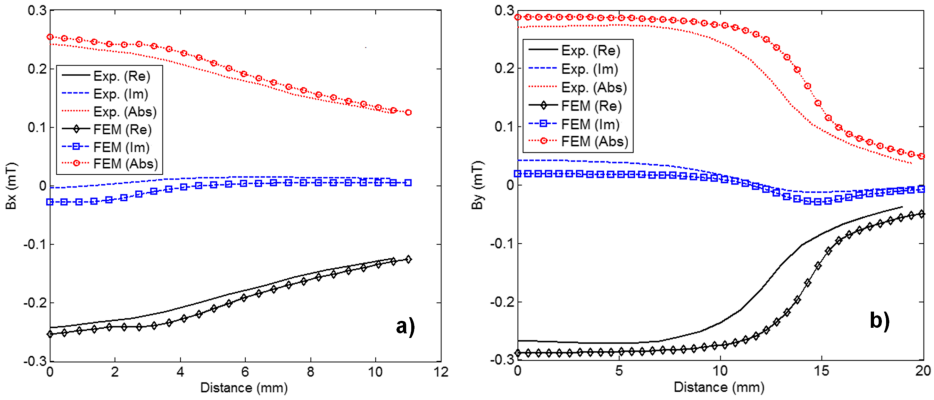

FIG. 6. Measured (Exp.) and FEM calculated magnetic flux density (tangential component) values on x-path (a) and on y-path (b) at 50 Hz - (Real values (Re), Imaginary values (Im) and absolute values (Abs)).

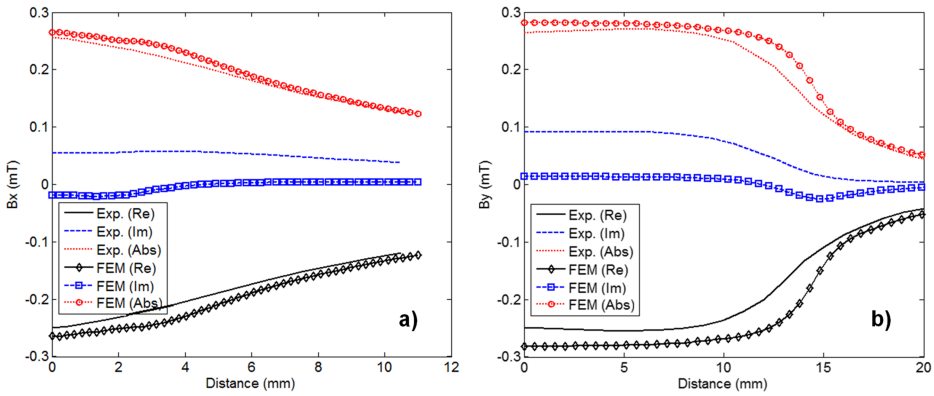

FIG. 7. Measured (Exp.) and FEM calculated magnetic flux density (tangential component) values on x-path (a) and on y-path (b) at 100 Hz - (Real values (Re), Imaginary values (Im) and absolute values (Abs)).

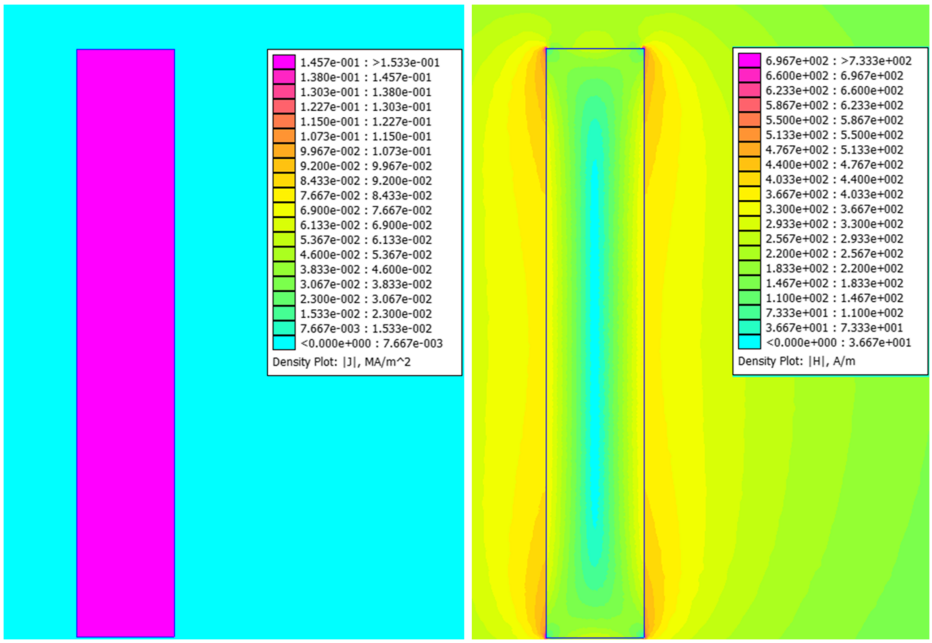

FIG. 8. Current density distribution in the conductor (left) and magnetic field strength distribution (right) at DC (I_{DC} = $23/\sqrt{2}$) A).

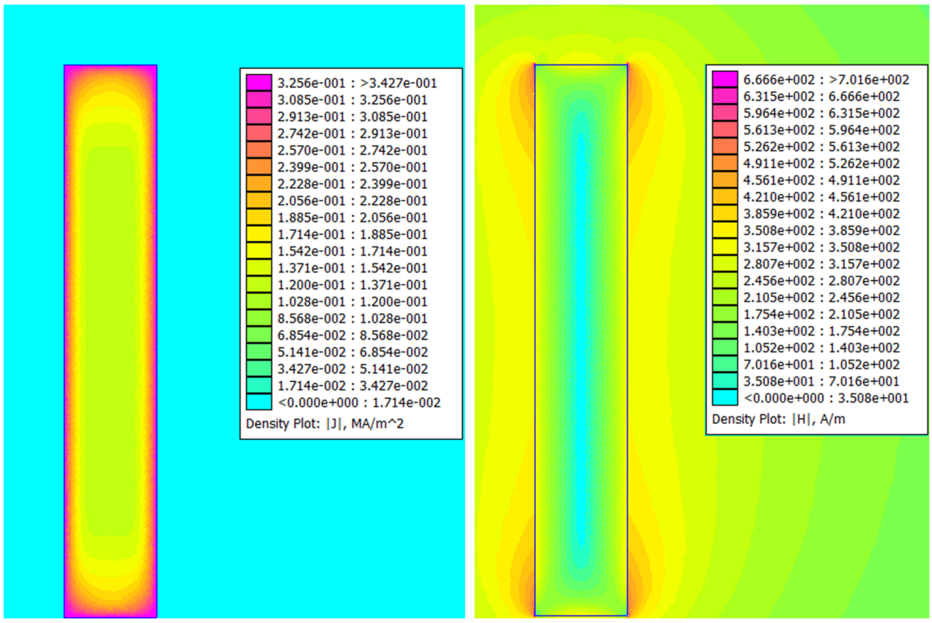

FIG. 9. Eddy current distribution in the conductor (left) and magnetic field strength distribution (right) at 50 Hz (I_{AC}=23 A).

of the busbar. This difference is increasing with reducing the distance and surprisingly it is slightly decreasing with frequency. The maximum difference of 33 % is observed at DC and in the minimum technically achievable distance of 1.5 mm. Increasing the distance to 6 mm reduces the maximum difference to 10%.

From the observed dependencies we may estimate that the main factor influencing the difference is busbar permeability, not the change between resistivity. The difference is decreasing with frequency, which indicates again that the effect of conductor permeability is stronger than the effect of eddy currents.

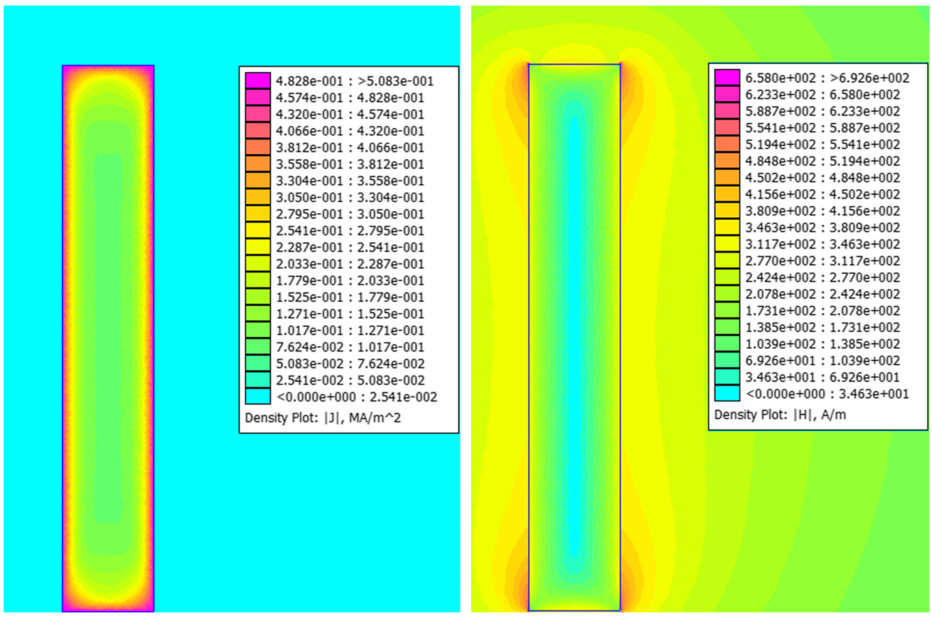

FIG. 10. Eddy current distribution in the conductor (left) and magnetic field strength distribution (right) at 100 Hz (I_{AC}=23 A).

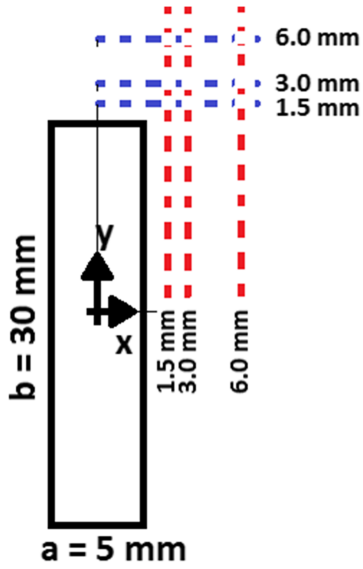

FIG. 11. Considered paths for magnetic flux densities (1.5 mm, 3 mm and 6 mm distances from the surface of conductor) - center of coordinate is located in the center of rectangular conductor.

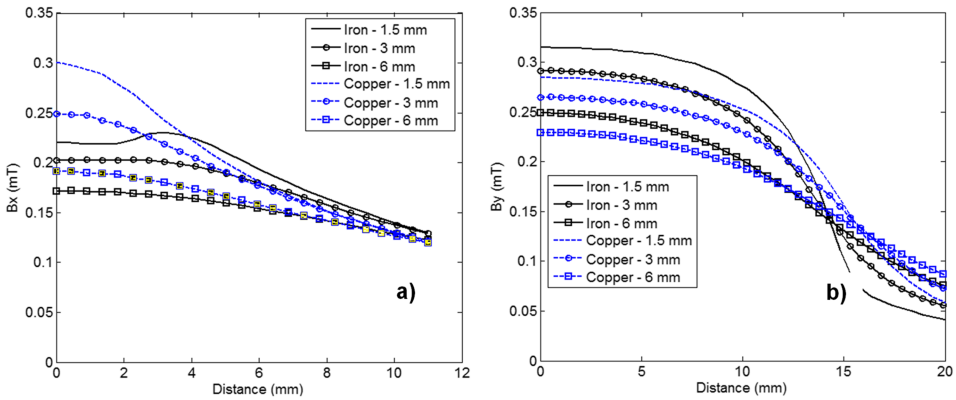

FIG. 12. Magnetic flux density (absolute value of tangential component) values at different paths (FIG. 11) using FEM at DC ($I_{DC} = 23/\sqrt{2}$ A) - x-directions (a) and y-directions (b).

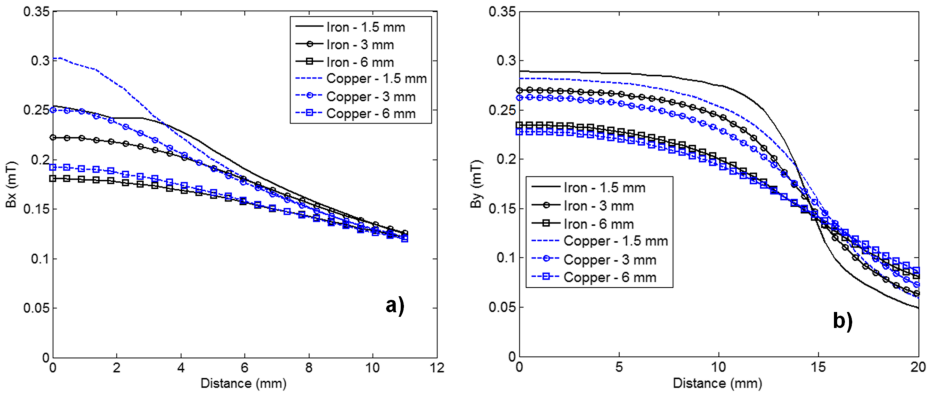

FIG. 13. Magnetic flux density (absolute value of tangential component) values at different paths (FIG. 11) using FEM at 50 Hz- x-directions (a) and y-directions (b).

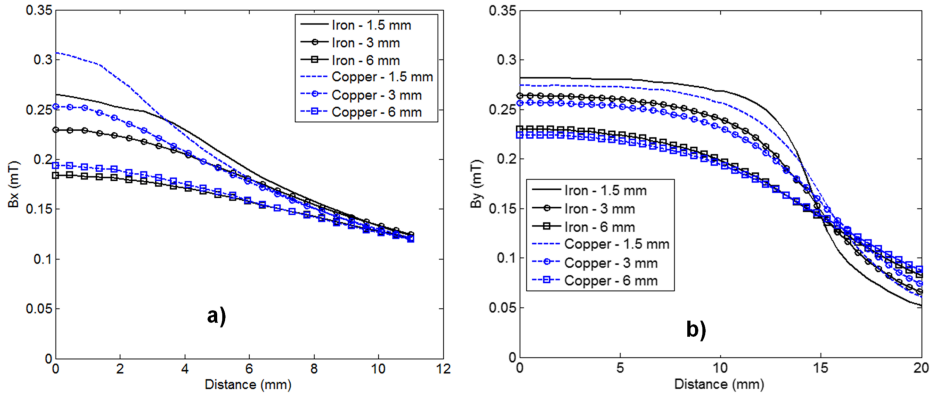

FIG. 14. Magnetic flux density (absolute value of tangential component) values at different paths (FIG. 11) using FEM at 100 Hz- x-directions (a) and y-directions (b).

IV. CONCLUSIONS

In this paper, measurement and calculations of magnetic flux densities around a rectangular conductor were presented. Solid iron and copper were used for conductor material. We measured the material properties to be used for FEM simulations and verified the fit with measured field values around the conductor. General conclusion is that yokeless current sensors cannot be used for iron busbars without recalibration. Maximum error caused by the busbar permeability is 33% at DC and in minimum distance between the sensor and the busbar. If the distance is increased to 6 mm, the error drops to 10 %. The error is slightly decreasing with frequency, indicating that the difference in resistivity between copper and iron is not the dominant source of the error.

ACKNOWLEDGMENTS

This work was supported by the Grant agency of the Czech Republic through the project "New methods for the measurement of electric currents" (GACR 17-19877S).

[1] P. Ripka, "Electric current sensors: A review," Meas. Science and Technology **21**(11), 1–23 (2010).
[2] Y.-P. Tsai, K.-L. Chen, Y.-R. Chen, and N. Chen, "Multifunctional coreless Hall-effect current transformer for the protection and measurement of power systems," IEEE Trans. Magn **63**, 557–565 (2014).
[3] M. Blagojevič, U. Jovanovič, I. Jovanovič, D. Mančič, and R. S. Popovič, "Realization and optimization of bus bar current transducers based on Hall effect sensors," Meas. Sci. Technol. **27**, 065102 (2016).
[4] P. Ripka, V. Grim, and V. Petrucha, "A busbar current sensor with frequency compensation," IEEE Trans. Magn. **53**(4) (2017), paper # 4000505.
[5] V. Frick, L. Hebrard, P. Poure, F. Anstotz, and F. Braun, "CMOS microsystem for AC current measurement with galvanic isolation," IEEE Sensors J. **3**, 752–760 (2003).
[6] P. Ripka and A. Chirtsov, Influence of External Current on Yokeless Electric Current Transducers, proc. Intermag 2017, accepted for IEEE Trans. Magn.
[7] L. Di Rienzo, R. Bazzocchi, and A. Manara, "Circular arrays of magnetic sensors for current measurement," IEEE Trans. Instrum. Meas. **50**(5), 1093–1096 (2001).
[8] K. L. Chen and N. Chen, "A new method for power current measurement using a coreless Hall effect current transformer," IEEE Trans. Instrum. Meas. **60**, 158–169 (2011).
[9] G.-J. Huang, N. Chen, and K.-L. Chen, "Self-calibration method for coreless Hall effect current transformer," 2016 IEEE Power and Energy Society General Meeting (PESGM), Boston, MA, 2016, pp. 1–5. Subm. To IEEE Trans. On Power Delivery.
[10] P. Mlejnek, M. Vopalensky, and P. Ripka, "AMR current measurement device," Sensors and Actuators A **141**, 649–653 (2008).
[11] R. Weiss, R. Makuch, A. Itzke, and R. Weigel, "Crosstalk in circular arrays of magnetic sensors for current measurement," IEEE Transactions on Industrial Electronics **64**(6) 4903–4909 (2017).
[12] D. Lee, M. Eissa, A. Gabrys, B. Shulver, E. Mazotti, S. Lavangkul, S. Chevacharoenkul, N. Murphy, F. Wang, Y. Zhang, W. French, M. Jenson, and R. Jackson, Fabrication and Performance of Integrated Fluxgate for Current Sensing Applications, Intermag 2017, in press IEEE Trans. Magn.,
[13] http://www.femm.info/wiki/Documentation/, accessed 2017/07/02.